International Journal of Rock Mechanics & Mining Sciences 80 (2015) 19–30

Contents lists available at ScienceDirect

International Journal of Rock Mechanics & Mining Sciences

journal homepage: www.elsevier.com/locate/ijrmms

Improvement of photogrammetric JRC data distributions based on parabolic error models

Dong Hyun Kim [a,*], George V. Poropat [b], Ivan Gratchev [a], Arumugam Balasubramaniam [a]

[a] School of Engineering, Griffith University, Gold Coast, QLD, Australia
[b] CSIRO Exploration and Mining, QLD, Australia

ARTICLE INFO

Article history:
Received 9 January 2015
Received in revised form
7 August 2015
Accepted 8 September 2015

Keywords:
Photogrammetry
JRC
Allowable distance
RMSE

ABSTRACT

This research describes the influences of the focal length of lenses as well as camera-to-object distances that control the accuracy and precision of 3D photogrammetry models used for assessing joint roughness coefficients (JRC). A parabolic error model, which is developed by a series of photogrammetric laboratory tests, is used to improve the JRC data distributions obtained from the photogrammetry 3D models. The influences of camera-to-object distances and focal lengths on the accuracy of JRC values are investigated in laboratory conditions. A series of photogrammetry tests are performed under different conditions by varying the camera-to-object distances and the camera lens focal lengths. The camera positions are controlled on a sliding device to increase the accuracy of geo-referencing. The results suggest the allowable photographic distances for the employed photogrammetry equipment (e.g. camera and focal lengths of lenses) to estimate JRC values through comparison with the manually measured values. The root-mean-square-error (RMSE) of JRC functions, which are correlated with the camera distances and the normalized JRC values, are depicted as different size parabolic curves according to the employed focal lengths. These models successfully improve on the accuracy of the originally obtained JRC distributions.

1. Introduction

The joint roughness coefficients (JRC) are important values to evaluate rock mass stability problems.[1,2] The values have been generally determined by manual measurements using profile gauges for joint surfaces of rock samples or rock masses. However, to achieve more accurate and to obtain more roughness data over larger and potentially inaccessible areas than manual measurements, remote sensing techniques such as terrestrial laser scanning (TLS) and close range photogrammetry (CRP) are also employed in both laboratory and site investigations.

TLS has been preferred to investigate JRC values compared to CRP.[3–11] This is due to the general recognition that TLS can produce higher accuracy and resolution images than CRP. However, it is difficult to disregard the significant advantages of photogrammetry which are portability, economic feasibility, legibility of visual information and convenience. Furthermore, it is considerably beneficial that photogrammetry is able to provide structured color images in which exposed joint surfaces can be distinguished from the excavated surfaces.

The applicability of photogrammetry to obtain rock joint surface roughness has been investigated through laboratory tests and site investigations.[12–18] Recent leading studies on the estimation of JRC from 3D digital photogrammetry models[19–25] suggest that high-resolution images are required to obtain reliable JRC values. In photography, it is generally expected that the measurement accuracy can be improved by increasing the focal length of lenses or decreasing photographic distances to the object. Poropot [22] conducted a series of laboratory tests for JRC estimation using low resolution level images with 2.5 mm pixel size at 100 m, using a 24 mm focal length lens. Kim et al.[24] extracted roughness profiles from a 3D photogrammetry model of a natural rock slope which was obtained using a commercial grade SLR digital camera with a 24 mm focal length lens in the distance range from 2 m to 10 m. In the results, it was found that the roughness profile discrepancies between the manual measurements and the photogrammetric 3D models increased, as the camera-to-object distances increased.

The resolution limits of remote sensing methods are an important factor in investigating rock surface roughness. In contrast with the considerable number of investigations for laser scanning methods, further investigation is required for photogrammetry methods. In manual measurements, profile gauges are used for obtaining roughness profiles at a fixed horizontal interval. The step sizes of the profile gauges normally range from 0.5 mm to 1.0 mm. It is reported that if the data interval is more than 1 mm, JRC values may be underestimated due to the reduced asperity angles for

* Corresponding author.
E-mail address: donghyun.kim@griffith.edu.au (D.H. Kim).

http://dx.doi.org/10.1016/j.ijrmms.2015.09.007
1365-1609/

the step sizes.[26] On the other hand, Poropot[21] emphasized the importance of understanding the measurement error for surface profiles corrupted by noise when using small pixels. The study attempted to filter the corrupted profiles with different window sizes. The results showed that JRC values can be properly estimated using filtering algorithms, when the measurement noise is significant in relation to the sample spacing. However, this distorted noise of individual asperities may still result in the overestimation of JRC values.

In actuality, many variables such as the camera-to-object distance, camera calibration, base-to-distance ratio, data noise, modeling algorithms, lighting and shadows can lead to data corruption in photogrammetry. Therefore, comparison cannot simply be made between image resolutions and the accuracy of JRC values, even in the idealized laboratory conditions (e.g. indoor lighting, accurate measurements). This study focuses on the influences of the camera-to-object distances and focal lengths on the precision and accuracy of JRC values. It can be generally accepted that large camera distances with short focal lengths contribute to producing large measurement errors and standard deviations for JRC estimations. This claim can be supported by the fact that cameras with longer focal lengths decrease measurement errors in stereo photogrammetry systems.[27]

In this study, the authors firstly present the allowable distances for photogrammetry to estimate JRC values based on the accuracy of manual measurements using a 1 mm step size. These distances were derived by performing a series of photogrammetry laboratory tests with three different focal length lenses over differing camera-to-object distances. In the whole test range of camera-to-object distances, the obtained photogrammetric JRC values showed large discrepancy between the estimated values and the manually measured values; however, a better performance could have been obtained by using the data from only within the allowable distance for each lens. Root-mean-square-error (RMSE) is used to measure the discrepancies between predicted values and measured values. Secondly, quadratic error equations describing the relationships between the RMSE of JRC and the normalized JRC values for different camera-to-distances are presented in this study. The quadratic functions are formed with different curvatures according to their focal lengths.

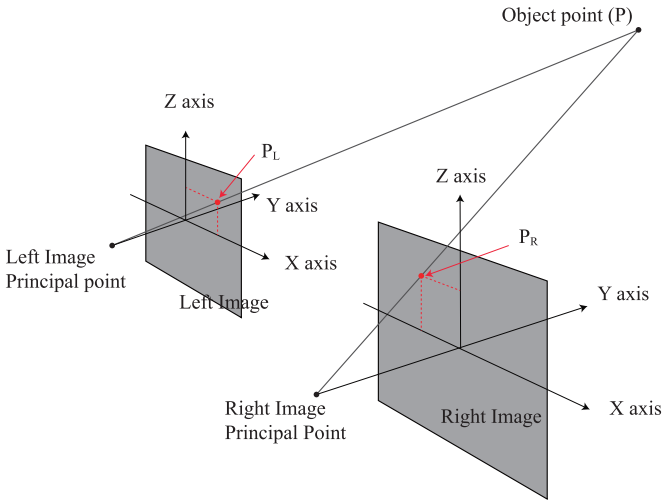

Fig. 1. Geometry for the determination of the position of a point in object space using photogrammetry.[23]

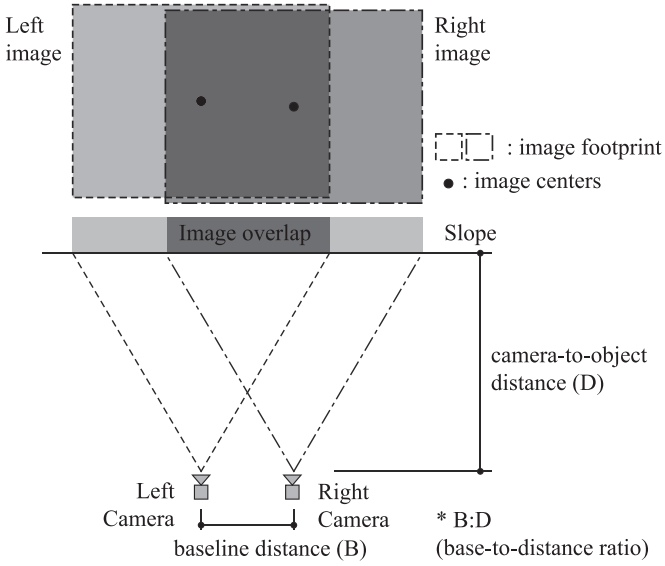

Fig. 2. An example of image capture setup for 3D model.

2. Principles of photogrammetry

The principle of photogrammetry is explained by the calculation of 3D coordinates based on the coordinates of images, employed camera parameters and ground control points.[28] This is explained as the concept of stereoscopic parallax, which is the position change of an object with respect to the changed camera locations as shown in Fig. 1. In the 3D coordinate system, the x coordinates of the point P on both images are different as P_L and P_R. Thus, the 3D position of the point P can be identified using relationships between the relative positions obtained from the images and the camera perspective center.

Photogrammetry creates 3D images using two or more images. Stereoscopic images are produced by taking two images from two different positions. 3D models are achieved from the overlapped area of both images. As demonstrated in Fig. 2, a slope surface can be photographed and the 3D image of the overlapped area is generated by photogrammetry programs. To obtain better models in a photogrammetry survey, the most effective photo layout for the area should be determined after the size and area of interest is established. In the matching process of photogrammetry, it is generally recommended that the overlapped portion of the images should be more than 25% of the image area when taking photographs[29] and moreover, the best stereo image pairs have an overlap range of 50–60%.

3. Systematic and measurement errors on photogrammetric JRC data

3.1. Influencing factors

In order to obtain reliable JRC data from photogrammetry, photogrammetry surveys often require the use of high-end cameras and longer focal length lenses to keep high spatial resolution. However, it has been recognized that there are other various influencing factors associated with the accuracy of 3D models. Recently, Dai et al.[30] reported that the measurement errors related to photogrammetry can be categorized by the following two aspects: one is due to bad planning of camera network geometry and the other is attributed to camera systems.

Image-based errors are introduced by inaccuracy in camera systems. Lens distortion is one of the most significant factors that can lead to systematic errors and needs to be taken into account for any photogrammetric application.[31] In case of the radial distortion of a single optical lens, the distortion effect is magnified

along the radial direction of the lens; thereby the sizes of the errors are dependent on the distance from the center of the images.[30] Currently, three representative commercial-grade digital photogrammetry packages (Sirovision (CAE), 3DM Analyst (ADAM Technology) and ShapeMetrix3D (3G Software and Measurement)) require periodic calibration of the employed lens and camera combination or support for the calibration in the camera and lens data.[32]

The depth accuracy of 3D images depends on the base-to-distance ratio. If the ratio is large, the depth accuracy of the 3D model can be increased. However, in a general photogrammetry setup for rock slope surveys, the large base distances of the stereo photographs result in two different views. This may lead to difficulty in recognizing common points in the matching process of photogrammetry.[33] Practically, photogrammetry programs recommend a desirable range of base-to-distance ratio ranging from 1:10 to 1:2[29,33] for rock slope surveys. The angle of incidence is the angle between the optical axis of the lens on a surface and the line perpendicular to the surface. It should be noted that this angle should be reduced to obtain accurate 3D models.[30] Orthogonal photographs are thus desirable for minimizing the image base errors.

In this experimental study, the employed lenses are fully compatible with the photogrammetry software, Sirovision. The calibrations of the employed lenses and camera body combinations are firstly performed by using the calibration data files supported by the manufacturer. The positions of the object in the images are also arranged to focus on the middle of the images to minimize the influence of radial distortion of the lenses. Secondly, with respect to the photogrammetry setup, the base-to-distance ratio is kept constant in the desirable range of Sirovision. Thus, the variations of depth accuracy according to the base-to-distance ratio are not addressed in this study. Thirdly, photographs are taken in the orthogonal direction for the sample surface; in so doing, the influence of the angle of incidence on the image base errors is reduced.

3.2. Estimation of measurement errors

In close range photogrammetry, an increase of camera-to-object distances to objects normally results in the reduction of data accuracy. In this case, the accuracy and precision of 3D photogrammetric coordinates can be analyzed by statistical approaches. In photogrammetric modeling, the procedure from data acquisition to analysis can be regarded as a process to create JRC values. Therefore, it is assumed that the obtained values contain random errors which can be caused by the main change (e.g. camera lenses) under identical photogrammetric survey conditions. In relation to JRC estimation, two parameters, which are the maximum asperity heights (H_a) and the estimated JRC values obtained from the extracted profiles of photogrammetric models, are employed to analyze the data accuracy.

The root-mean-square-error (RMSE) is defined to be the square root of the average of the squared discrepancies. The RMSE values of coordinates are employed to check the accuracy of the surveyed data in photogrammetric 3D models.[34] In this study, the RMSEs in the maximum asperity heights and estimated JRC values are used for describing the accuracy of photogrammetric roughness profiles as estimated by

$$\mathrm{RMSE}_{Ha}=\sqrt{\frac{\sum_{i=1}^{n}(H_{o,i}-H_{p,i})^2}{N}} \tag{1}$$

$$\mathrm{RMSE}_{JRC}=\sqrt{\frac{\sum_{i=1}^{n}(\mathrm{JRC}_{o,i}-\mathrm{JRC}_{p,i})^2}{N}} \tag{2}$$

where H_o and JRC_o are the manually measured values of asperity height and JRC values; and H_p and JRC_p are the values of asperity height and JRC values obtained from the photogrammetric models of each profile. Comparing the JRC values obtained from the 3D models with those from manual measurements, the normalized values, N_{JRC} in Eq. (3), provides an indication of the accuracy of the photogrammetric models compared to manual measurements.

$$N_{JRC}=\frac{\mathrm{JRC}_{3D\ images}}{\mathrm{JRC}_{measured}} \tag{3}$$

3.3. A measurement error model factored by lens focal length and camera-to-object distances

In the relationships between image scales and focal lengths of lenses, it is known that higher measurement precision can be achieved by longer focal lengths with a reduction in the range of measurement errors.[27,35] Thus, it can be demonstrated that the measurement data histograms obtained by longer focal length lenses have narrower distribution widths than those obtained by lesser focal length lenses. The widths of the distributions, which represent the precision of data, can be expressed by the values of standard deviation as shown in Fig. 3.

To obtain JRC values from rock slopes, an increase of focal lengths can be required as part of the photogrammetry setup to improve measurement precision of the 3D coordinates. However, an increase in focal length may not be exactly proportional to the measurement accuracy and precision. This is due to the fact that different accompanying factors can also affect the accuracy of the results, as introduced in Section 3.1.[30]

In this study, an error model is introduced to characterize the influence of the image scale modification related to lens focal length and camera-to-object distances on the accuracy of JRC estimates. It will be mentioned in the following sections of this article that the distributions of the RMSE of the roughness data fit parabolic curves. The RMSE data (RMSE_{JRC} and RMSE_{Ha}) for given camera-to-object distances formed quadratic functions using the normalized JRC values. The following basic quadratic function is proposed:

$$\mathrm{RMSE}_{JRC}\cdot d=aN_{JRC}^2+bN_{JRC}+c \tag{4}$$

where d represents the camera-to-object distance; a is a coefficient to determine the direction and the size of the parabola which represents the precision of the data; and b and c are the coefficients to determine the locations of the vertex of the

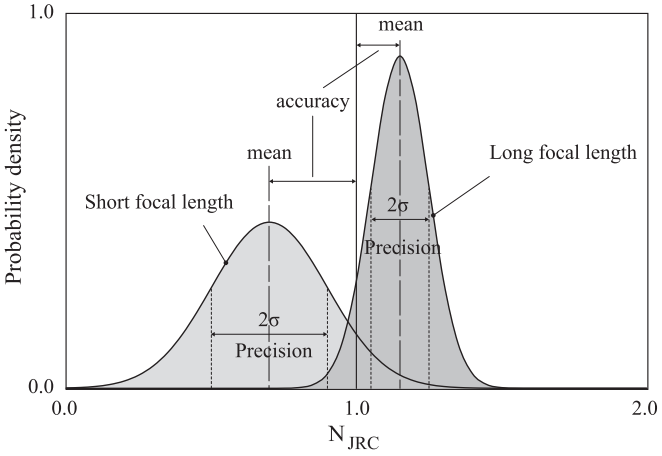

Fig. 3. Concept of measurement precision according to lens focal length.

parabola. In this quadratic model, the coefficients are easily interpretable. The proposed quadratic functions all have the same basic "U" shape. It is interesting that the widths of the upward parabolas vary with the employed focal length of lenses. Larger focal lengths create steeper curves with narrower widths than short focal lengths. The widths of the parabolas are expressed by the values of the coefficient '*a*' of the equations. Because the *x*-coordinate of the vertex of the parabola is located near the point N_{JRC}=1, the coefficient *b* can be approximately correlated with the coefficient *a* as follows:

$$b \cong -2a \tag{5}$$

The coefficient, *c*, is the average value of $RMSE_{JRC} \cdot D$ when the estimated JRC value is '0'.

4. JRC estimations

4.1. Maximum asperity height

For the first order asperities: large scale roughness, lengths of profiles and maximum amplitude values of digitized asperity data can be used to determine JRC values. The empirical JRC chart,[1] as shown in Fig. 4, supporting the straightedge method may not be so strict for the accuracy of the digitized profiles compared to the mathematical methods that are described in the following section. In accordance with this advantage, JRC values have been estimated by using the straightedge method based on 3D surface data. As a similar study, it was reported that a 3D scanning image was used for estimating JRC values by the straightedge method within a close range (3 m away from a rock surface). The study showed that there are minor differences in JRC values between manual measurement and laser scanning.[11] Recently, using 3D images, the maximum asperity values of the roughness profiles have been also

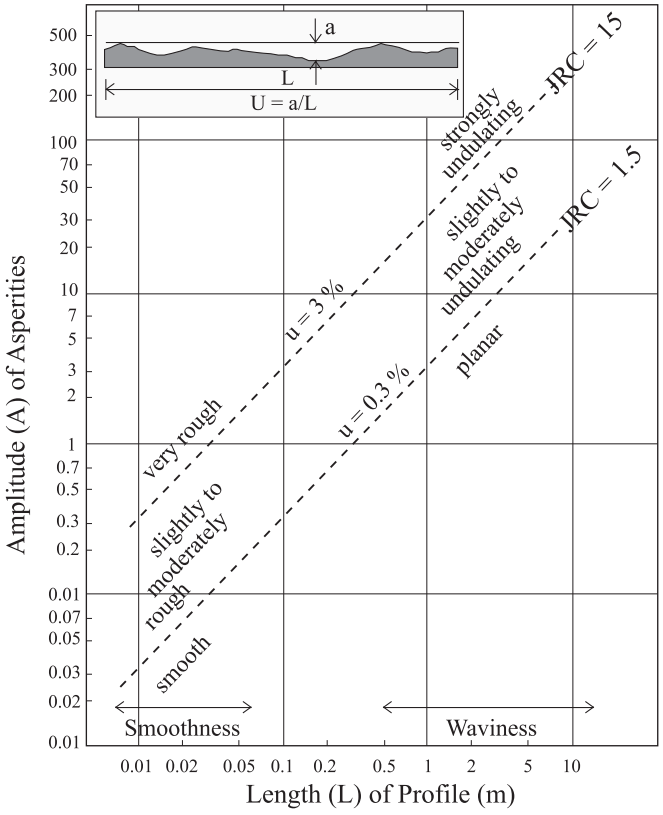

Fig. 4. Joint waviness and smoothness.[36]

Table 1
Experiment device details for photogrammetric experiment.

Device	Values
Camera model	Nikon D7000
Sensor size	23.6 mm × 15.6 mm
Resolution	4928 × 3264 Pixels
Pixel size of sensor	4.78 μm
Lenses/view angles (deg)	AF Nikkor 24–85 mm f/3.5–4.5G [24(fixed)]/61.0 AF Nikkor 50 mm f/1.8D/31.3 AF Nikkor 85 mm f/1.8D/18.5

employed to quantifying JRC values based on PalmstrÖm's RMi system.[36–38]

4.2. Digitized profile coordinates

The mathematical expressions of joint roughness have been investigated using various parameters. In two dimensional profile analyses, roughness parameters, which characterize surface topography based on amplitudes and horizontal characteristics of the surface deviations, have been used to establish correlations between the parameters and JRC values.[39–44] For the second order asperities: small-scale roughness parameters are calculated using the photogrammetry profiles to verify the roughness based on photogrammetry.

As a representative roughness parameter, Z_2, which shows strong correlations with JRC values, has been employed to estimate JRC values based on digitized roughness data. Tse and Cruden[39] established a regression equation using Z_2 to estimate the JRC of rock joint roughness profiles:

$$Z_2 = \left[\frac{1}{M(D_x)^2} \sum_{i=1}^{M} (y_{i+1} - y_i)^2 \right]^{1/2} \tag{6}$$

$$\mathrm{JRC} = 32.2 + 32.47 \log Z_2 \tag{7}$$

where *M* is the number of intervals, D_x is a constant distance lag and the sum of the squares in adjacent *y*-coordinates is divided by the product of the number of intervals. This parameter is however, varied with the step sizes (D_x) of asperities as shown in Eq. (6). Thus, the following different ranges of equations can be also used to take account of influence of measurement scales[43]:

$$\mathrm{JRC} = 60.32 Z_2 - 4.51 \quad \text{(for sample interval = 0.25 mm)} \tag{8}$$

$$\mathrm{JRC} = 61.79 Z_2 - 3.47 \quad \text{(for sample interval = 0.5 mm)} \tag{9}$$

$$\mathrm{JRC} = 64.22 Z_2 - 2.31 \quad \text{(for sample interval = 1.0 mm)} \tag{10}$$

5. Laboratory tests

5.1. Test setup

A single lens reflex digital camera (Nikon D7000), which has a high resolution CCD sensor (4928 × 3264 pixels), was employed to capture images of a rock sample. In order to obtain images with different resolutions, photographs of the rock sample were taken in the distance range of 1.0–7.0 m, spaced 0.5 m apart, using three different focal length lenses: FL=24 mm, 50 mm and 85 mm as shown in Table 1. Therefore, these photogrammetric tests were performed for thirty six different conditions. A sliding device, which is composed of two steel pipes (D=19 mm) and a moving

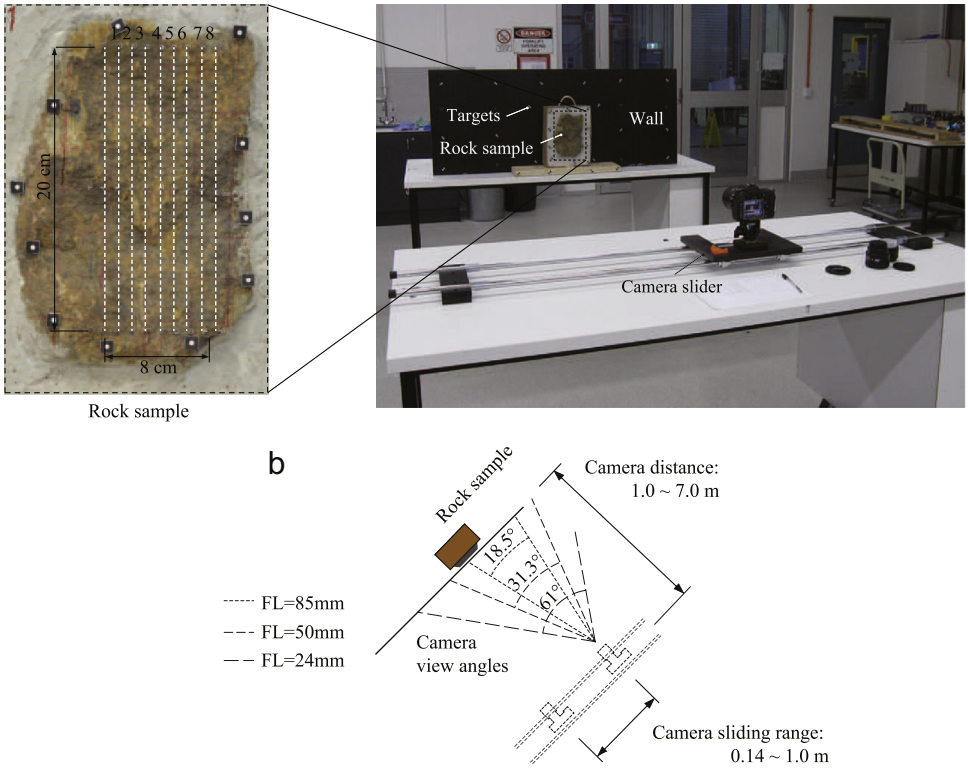

Fig. 5. Laboratory test setting, overview and rock sample (a) and view angles with focal lengths of lenses (b).

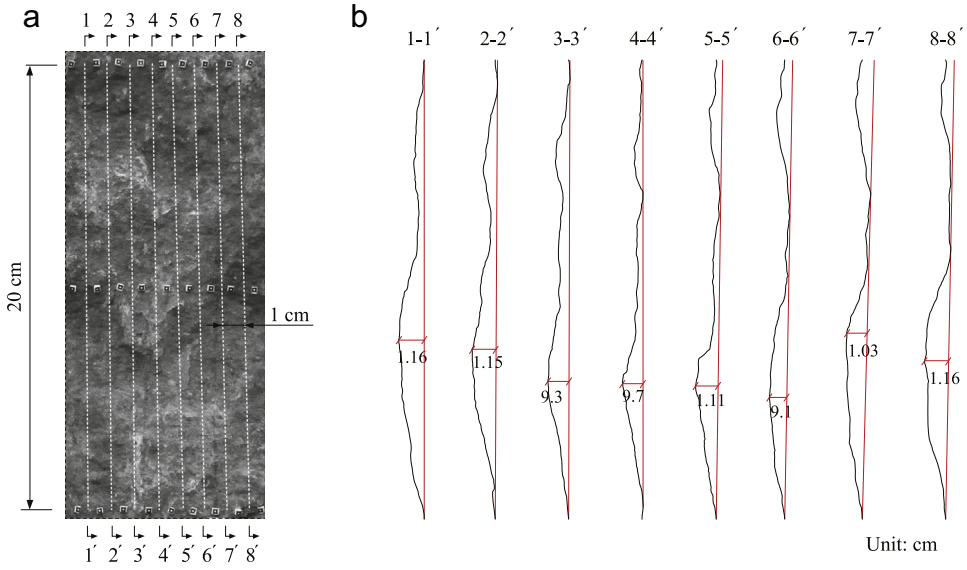

Fig. 6. Target area, measurement sections (a) and manually measured profiles at 1 mm intervals (b).

Table 2
JRC and H_a values of profiles.

No. profiles	1–1′	2–2′	3–3′	4–4′	5–5′	6–6′	7–7′	8–8′
JRC_o	10.2	11.0	9.9	11.5	13.5	10.7	10.7	10.9
H_o (mm)	11.6	11.5	9.3	9.7	11.1	9.1	10.3	11.6

plate with PVC pipe brackets to guide the pipes, is used to control the camera positions for the test conditions (Fig. 5). This device effectively increases the accuracy of distance measurement between the camera locations and the object for the various test conditions. As the height of the camera position is located on the same horizontal plane as the sample, image noise due to any occlusions of asperities can be minimized.

As the accuracy of the photogrammetry 3D models can be dependent on the lighting condition at the photograph moment,[18] all stereo photographs keep the same indoor lighting conditions in the laboratory. The computer code "Sirovision" version 5 (CAE) is used to create 3D images and extract roughness profiles. Generally, a decrease of the base-to-distance ratio can reduce the 3D image precision.[35] In this study, the base-to-distance ratio is fixed at the ratio of 1:7 on the basis of the desirable range of the Sirovision.[29] Geo-referencing is the process of locating and scaling digital images in a required coordinate system. In this study, the 3D images are referenced using the values of base distances of camera positions, and checked by comparing the distances of

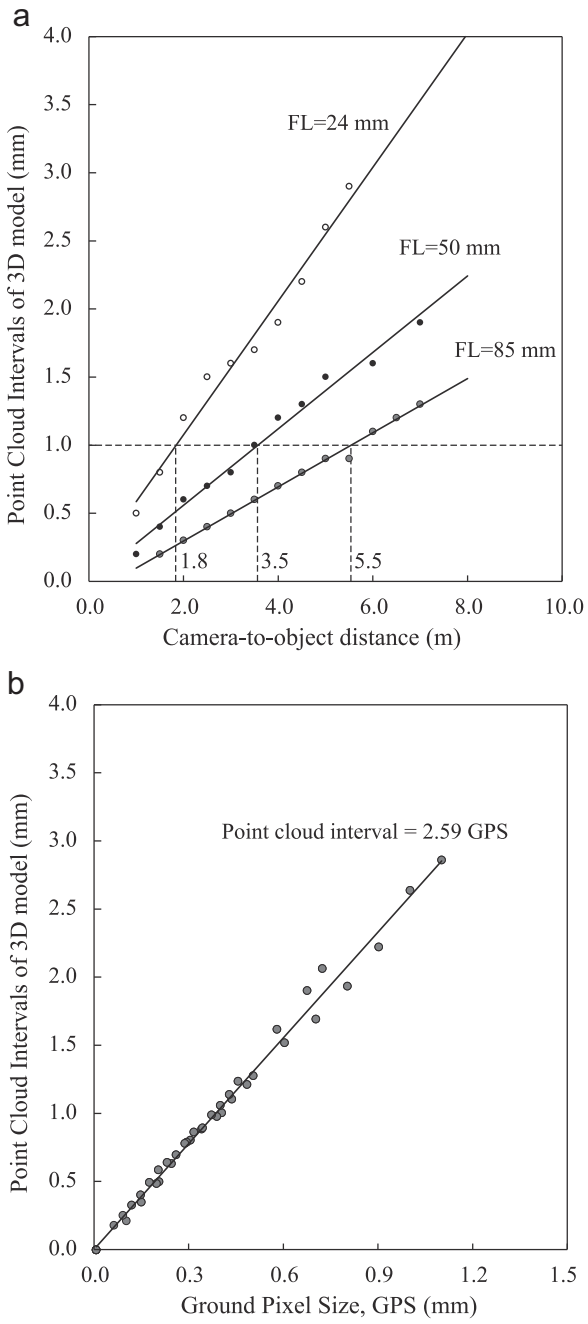

Fig. 7. Relationship between point cloud intervals and camera-to-object distances with focal length of lenses (a) and GPS (b).

the targets on the 3D models and the true distances to the sample. The accuracy of geo-referencing was within an error tolerance of 0.5%.

The sample is a weathered sandstone block which is embedded in cement plaster to keep it standing during the experiment as shown in Fig. 5. The length and width of the targeted area on the rock surface are 200 mm and 80 mm, respectively. The sample is positioned in front of a black panel on which black and white targets with a length of 1.5 cm are attached. For eight sections on the sample, roughness profiles are measured by a profile gauge (L=250 mm) at 1 mm intervals and the coordinates of the measured profiles are digitized using AutoCAD (Fig. 6). Table 2 shows the JRC values obtained from (Eqs. (6) to 10) and the measured maximum asperity height of each profile.

5.2. Measurement scales

The pixel size of an image is directly related to the intervals of point clouds, which indicate the measurement scales of photogrammetry profiles. As shown in Fig. 7(a), the point cloud intervals are simply increased with the camera-to-object distances and decreased with the values of focal length of lenses. Thus, the required maximum photographing distances can be obtained through simple relationships. For example, an FL=85 mm lens produces 1 mm interval 3D data clouds at a 5.5 m camera-to-object distance. These linear relationships can be combined using the ground sample distance (GSD) values which indicate the resolutions of the original images (Fig. 7(b)). The values are simply expressed by a function of the focal length, f, camera resolution (4.78 μm for Nikon D7000) and the camera-to-object distance, d, defined as[45]

$$\text{GDS} = \frac{d}{f} \times \text{camera resolution} \tag{11}$$

Thus, it can be said that in this laboratory condition, the images used to create 3D images have resolution that is 2.6 times denser than required.

6. Estimation of surface roughness

6.1. Maximum asperity heights

The spatial data of the 3D surface images were created using the photogrammetry code, Sirovision. The spatial data were then imported into AutoCAD which was capable of exporting two dimensional coordinates along the eight measurement directions from the 3D meshes. A total of 215 joint roughness profiles were extracted. The extracted profiles from the 3D images were visually compared with the shapes of roughness sections measured by a profile gauge (L=200 mm, 1 mm interval). Maximum asperity heights, H_a, were estimated using the highest and lowest values of asperity heights. Comparison of these values obtained from the photogrammetric models to the true values obtained from the measured profiles can measure the accuracy of the 3D surface models for the large scale roughness.

Fig. 8 compares the obtained profiles according to the sampling intervals and the focal length of the lenses for two representative sections. The vertical scale was exaggerated up to three times for clarity. Fig. 8(a) shows simulated profiles which were generated using 400 data points (0.5 mm intervals) and (b) demonstrates profiles with 1.0 mm intervals. It is noticeable from the results that the undulation geometries of the extracted profiles from the 3D images are similar to the true roughness profiles. However, to some extent, there are discrepancies in the second order asperities. Furthermore, the disparities tend to become more frequent in lower scale images, thus indicating the accuracy as well as precision in the 3D models is reduced.

It is interesting that the distance to the object is a critical factor to obtain accurate 3D surface models, even the 3D surface models using the same data intervals. Fig. 9 shows the variations of the maximum asperity heights, H_a, according to the ranges of the lenses. Even though the resolutions of the 3D images are kept constant, the H_a values are reduced with the increase of focal lengths. In other words, the accuracy of the photogrammetric 3D models is strongly affected by the camera-to-object distance.

6.2. JRC estimation and allowable distances for photogrammetric JRCs

Using the profile coordinates obtained from the 3D models, JRC values were estimated using Eqs. (6)–(10) (see Table 2). The manually measured profiles were digitized with a step size of 1.0 mm with the same intervals as the profile gauge and the JRC

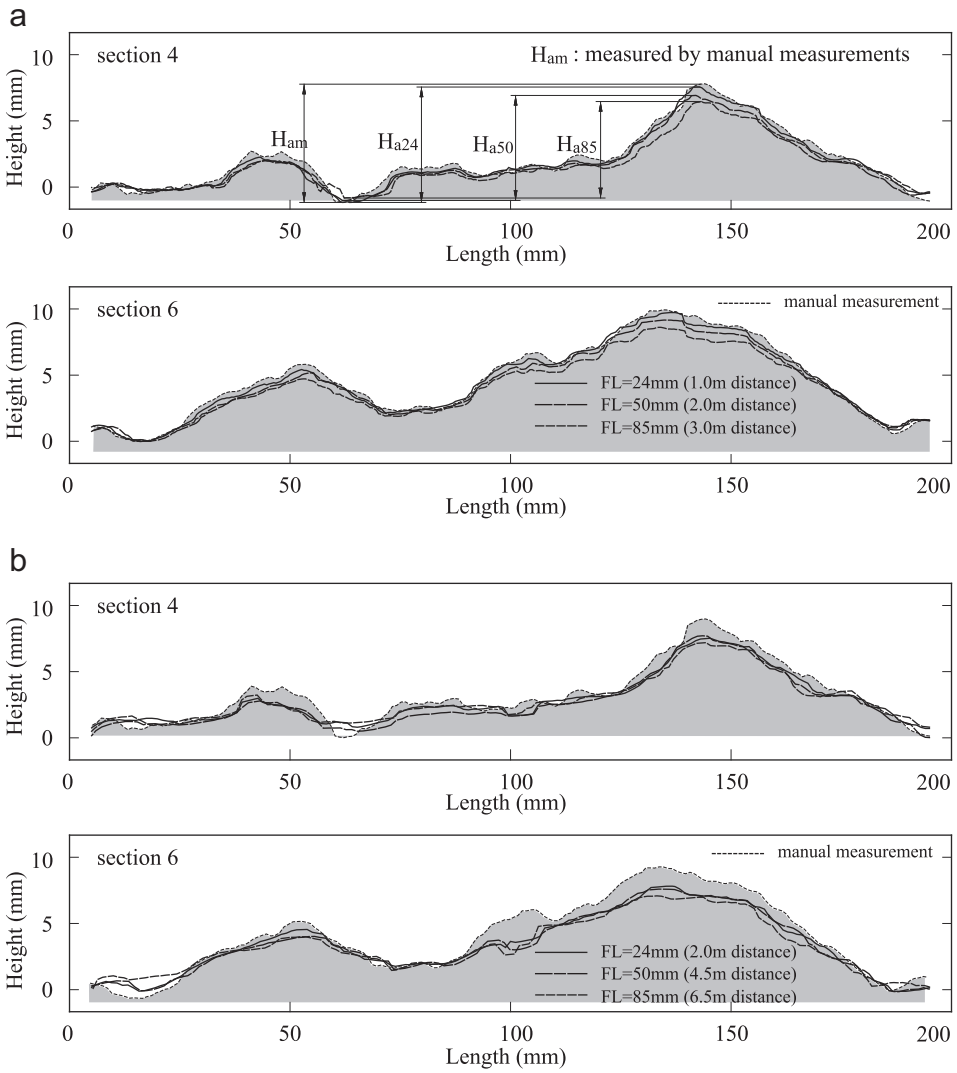

Fig. 8. Comparison of roughness profiles obtained from 3D images, 0.5 mm data intervals (a) and 1.0 mm data intervals (b).

values were calculated using the coordinates as well. The normalized values, N_{JRC} were then obtained using Eq. (3). All the JRC values obtained from the eight sections were statistically analyzed as shown in Fig. 8.

Exponential curves are adopted as the best fit for the decrease with increasing distances to objects. The data distributions are scattered for the various factors mentioned in the introduction. Based on the coefficient of determination, R^2 of Fig. 10, it can be said that the data ranges from 32% to 48% of the N_{JRC} values fit the linear relationships with the camera-to-object distances. However, the JRC values obtained from the 3D models obviously indicate downward trends as the camera moves farther from the rock sample, corresponding to the decrease of image resolution as presented in Fig. 10. Using the regression curves, intersections between the regression curves and the lines of $N_{JRC}=1$, indicate the allowable distances, d_a, which represents the threshold between over and under estimation of JRCs for each lens. For the wide angle lens (FL=24 mm), the calculated JRC values radically decrease with increasing camera distance. In other words, underestimation is obvious in the entire measurement range where the distance is over 1.0 m. In the case of 50 mm and 85 mm lenses, the allowable distances can be assumed as 2.0 m and 4.0 m, respectively. Table 3 shows the allowable distances obtained from the experiments. These distances are less than the distances that create 1 mm point cloud intervals for each lens (see Fig. 7(a)).

7. Statistical analysis

7.1. Measurement errors

The RMSE values determine the accuracy of the maximum asperity heights of simulated profiles which may indicate the accuracy of the coordinate systems of the 3D models (Table 4). It is difficult to find any interesting trends from the RMSE of the maximum asperity heights according to the differences of focal lengths. The values are similar for the three employed lenses. However, for the $RMSE_{JRC}$ values, the macro-lens (FL=24 mm) produced larger values than other lenses. It can be explained by the results that $RMSE_{JRC}$ values are more sensitive to the point intervals than $RMSE_{Ha}$ values within the test distances. It can be also noticed that the $RMSE_{JRC}$, which were estimated from the data using the three focal length lenses at the allowable distances, were considerably reduced to 1.73.

The normalized JRC values are plotted in the histograms and probability density plots of Fig. 11. With the assumption that the data fit the Gaussian distribution, the probability of N_{JRC} can be estimated. Fig. 11(a) shows that there is a 60% chance for obtaining the accuracy of JRC values within $\pm 20\%$ of standard deviations for all data set with the mean value ($\mu=0.87$) of N_{JRC}. In contrast with the complete data sets, the probability density function (PDF) formed by the data at the allowable distances, shows higher

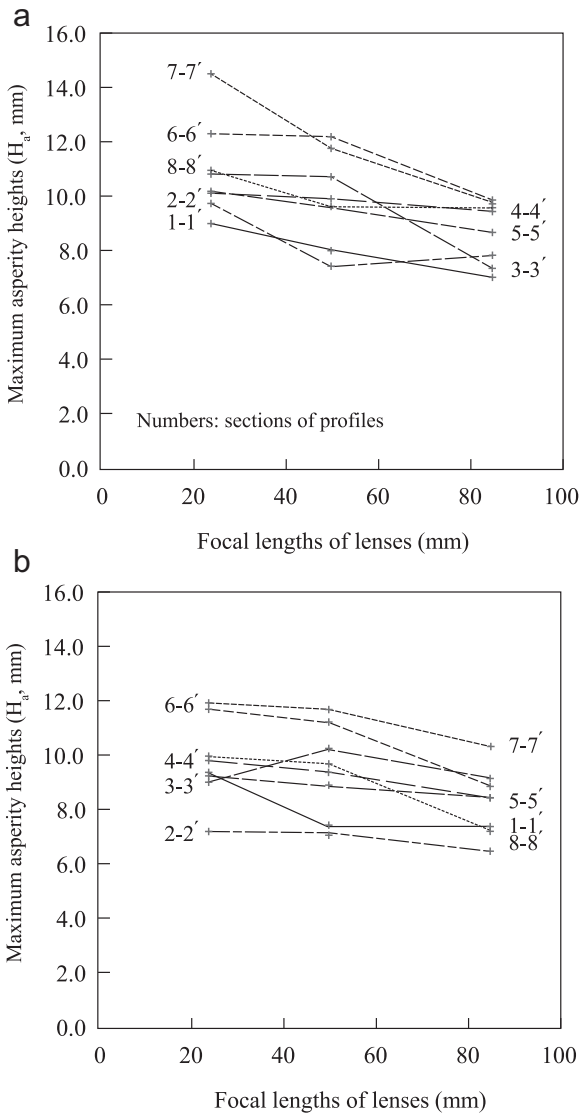

Fig. 9. Variation of the maximum asperity heights, H_a with focal lengths, pixel size = 0.5 mm (a) and pixel size = 1.0 mm (b).

probability (PDF = 0.85) of N_{JRC} and reasonable mean values (μ = 0.97) than does the entire data sets.

7.2. Proposed quadratic function of $RMSE_{JRC}$

The relationship between $RMSE_{JRC} \cdot D$ and N_{JRC}, which is analyzed for each focal length, presented good agreement (R^2 = 0.88–0.90) to a quadratic equation as shown in Fig. 12. The quadratic regressions are centered by N_{JRC} = 1 at their vertices. As mentioned in Section 3.3, the steepness of the sides of the parabolas and their concavity are controlled by the value of a, the coefficient on the x^2 term in its equation. This value increases as longer focal length lenses are employed and the widths of the parabolas are reduced, as presented in Table 5. It was also observed from the data distributions that the $RMSE_{JRC}$ values increased with increasing camera-to-object distances and the rates of increases were dependent on the focal lengths of the employed lenses.

Fig. 13 demonstrates exponential regression curves obtained from mean values of $RMSE_{JRC} \cdot D$ at a varying measurement distances for each focal length lens. The relationships indicate that $RMSE_{JRC}$ values are proportional to the camera-to-object distances.

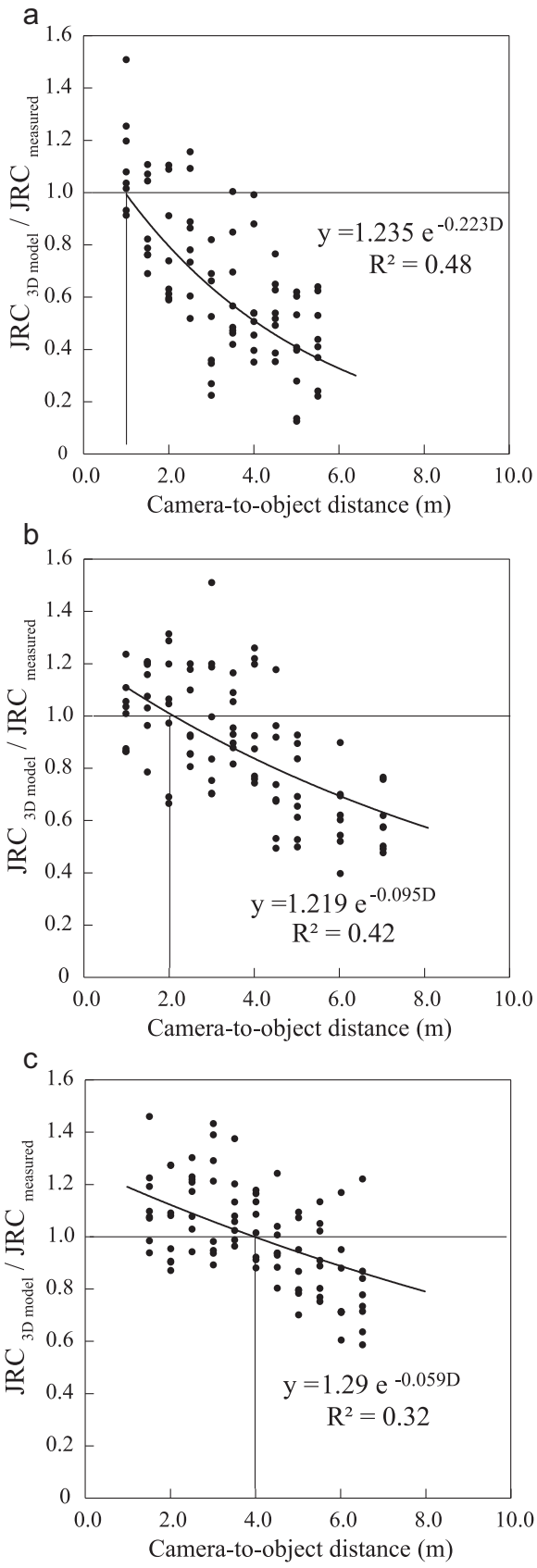

Fig. 10. Relationship between normalized JRC values and camera-to-object distances with different focal length lenses, FL = 24 mm (a), FL = 50 mm (b), and FL = 85 mm (c).

Table 3
Comparison of the allowable distances (d_a) for JRC estimation.

Focal lengths (FL, mm)	Camera distances to object at GPS=1.0 mm (m)	Experiment data	
		d_a (m)	Scale (d_a/FL)
24	1.8	1.0	41.7
50	3.5	2.0	40.0
85	5.5	4.0	47.1

Table 4
Error estimation for maximum asperity heights and JRC.

Focal lengths (mm)	Data number	$RMSE_{Ha}$ (mm)	$RMSE_{JRC}$
24	79	2.57	3.68
50	68	2.62	2.23
85	68	2.59	2.24
24, 50, 85	24 (Allowable distances)	2.32	1.73

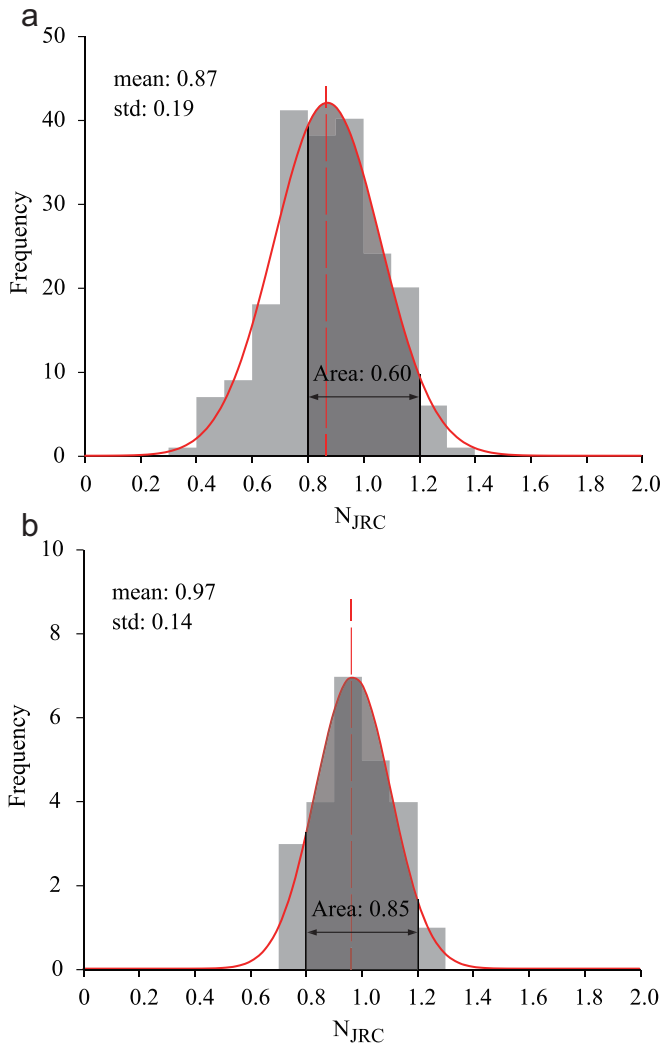

Fig. 11. Histograms and probability density functions of normalized JRC values in the entire ranges (a) and at the allowable distances (b).

However, it was also found that there was less agreement in the data for 85 mm focal length lenses (R^2=0.43) relative to that for 24 and 50 mm focal length lenses.

Using the mean values of $RMSE_{JRC} \cdot D$ for close distance ranges obtained from Fig. 13, the ranges of normalized JRC values can be

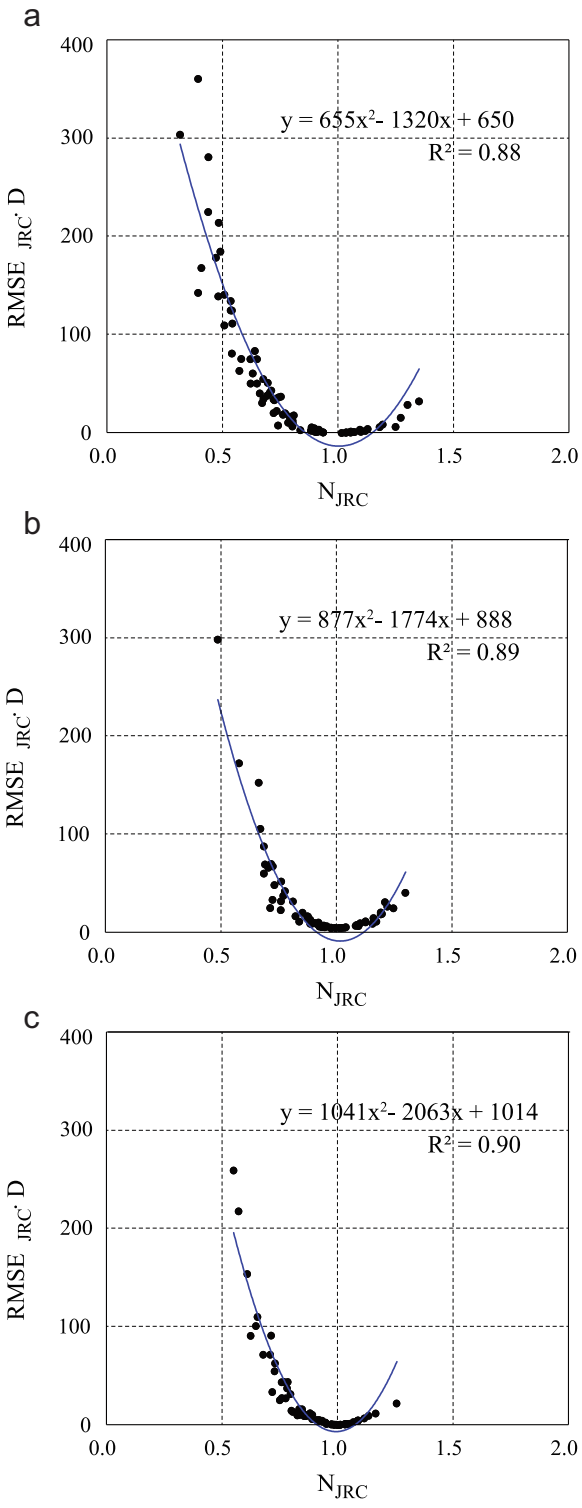

Fig. 12. RMSE distributions according to distances based on normalized JRC, FL=24 mm (a), FL=50 mm (b), and FL=85 mm (c).

Table 5
Coefficients of $RMSE_{JRC}$ quadratic equations according to focal length of lenses.

Focal length of lenses (mm)	*a*	*b*	*c*
24	655	−1320	651
50	877	−1774	888
85	1041	−2063	1014

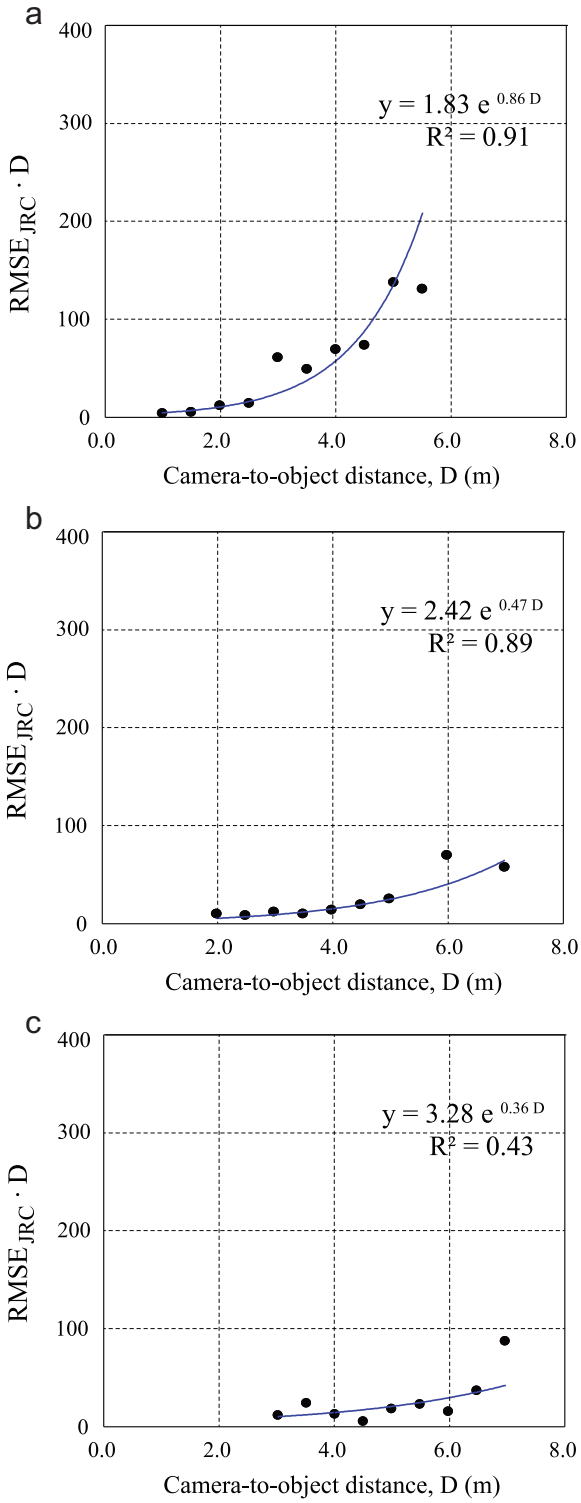

Fig. 13. Regression curves using mean values of $RMSE_{JRC}$ data obtained from each camera-to-object distance based on FL=24 mm (a), FL=50 mm (b), and FL=85 mm (c).

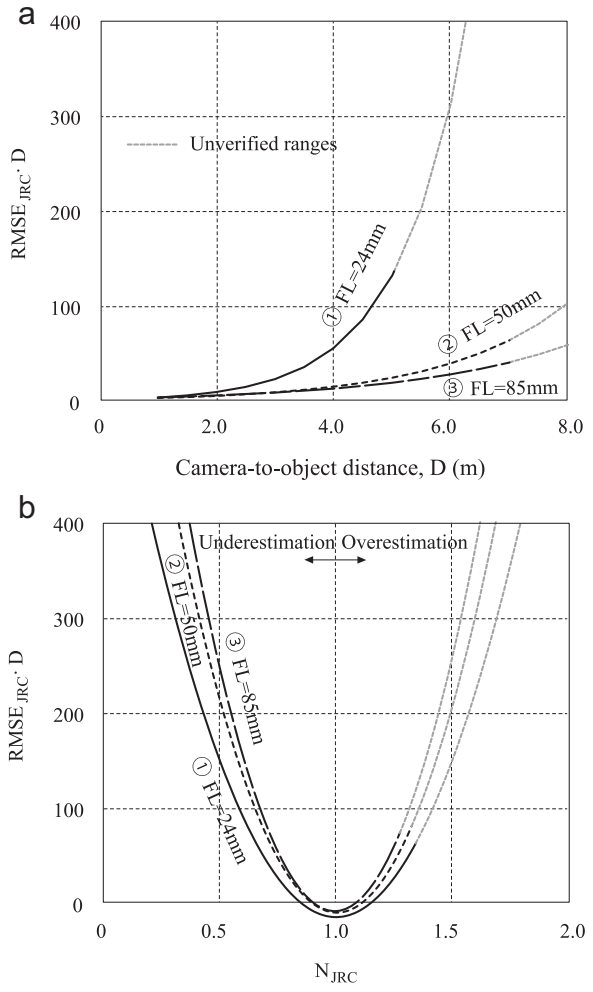

Fig. 14. RMSE parabola models based on focal lengths.

approximately predicted by means of the correlations between the parabola equations and the exponential regression curves as shown in Fig. 14. The camera-to-object distance ranges, which are used for the approximations, are also within the simulated distance range of up to 7.0 m. In terms of the feasibility of this method, the interpolation should be limited to the verified data ranges. When N_{JRC} values are over 1.3, these data ranges, which are drawn with dot lines in Fig. 14, are not verified. In addition, the upward trend of the parabolas, which turns up in the N_{JRC} ranges between 1 and 1.3, is due to the overestimated JRC values at closer distances for each focal length lens (see Fig. 8). Thus, the interpretation of the parabola equations in this study are applicable to the underestimated ranges less than $N_{JRC}=1.0$. In addition, it is worth mentioning that the parabola models were developed under ideal laboratory conditions. For practical purposes, the models can be improved by further studies using site photogrammetry data.

The histograms of N_{JRC} values obtained from the original data for each focal length lens provide reasonably distributed values with normal distribution shapes centered by $N_{JRC}=1.0$, as shown in Fig. 15. From the probability data functions, it is assumed that the precision of data can be indicated by the values within the standard deviation (σ) of the distributed data. Based on the influence of the camera-to-object distance, the mean values of N_{JRC} distributions for each focal length of lens were underestimated ranging from 0.78 to 0.93. The data are spread out from the mean values with the standard deviations from 0.15 to 0.23 as shown in Table 6.

Data reconciliation, using the quadratic equations (see Fig. 12), was able to improve the accuracy and precision of JRC data distributions by adjusting the initially biased JRC data. The redistribution of JRC values was performed by adding or subtracting the errors, which were estimated from the parabola equations, to the original JRC data. Fig. 15 compares JRC distributions between the original data and the reconciled data. The results indicate that the data reconciliation using the parabola error models for each focal

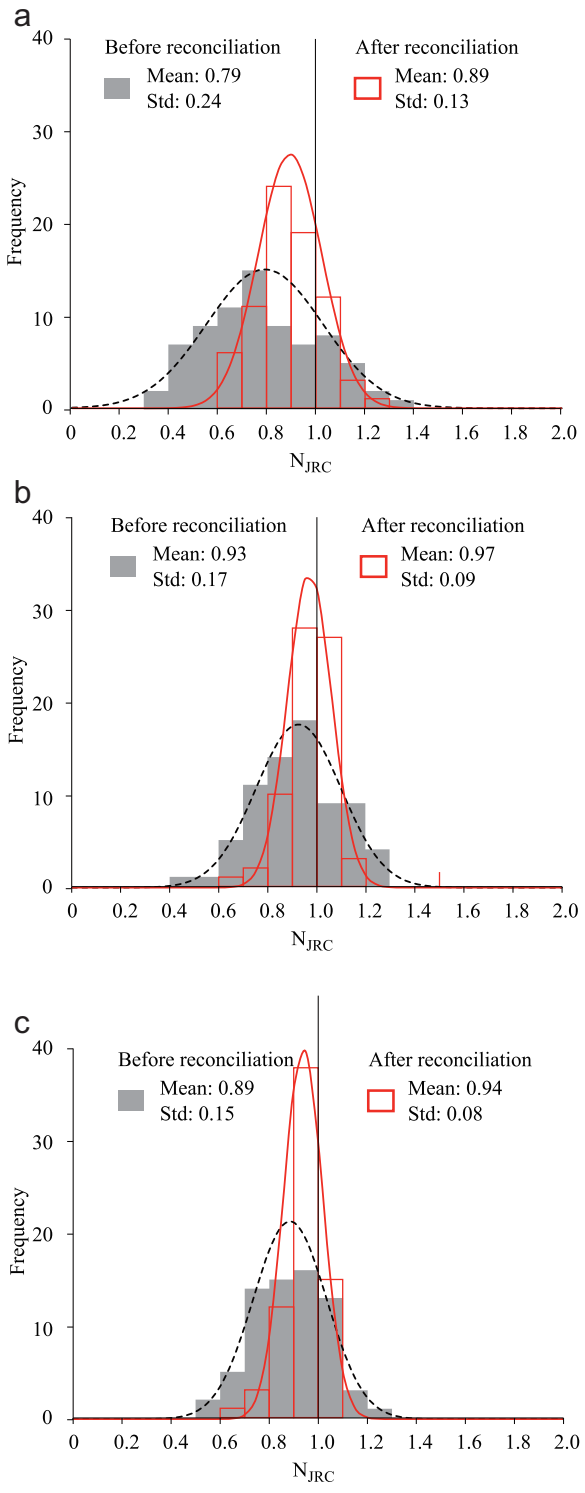

Fig. 15. Comparison of histograms and PDF between initial N_{JRC} data and updated N_{JRC} data, FL=24 mm (a), FL=50 mm (b), and FL=85 mm (c).

length lens effectively shifts the mean values to the true values and improves data precision.

The differences between the mean and standard deviation before and after the data reconciliation verify the effect of the parabola error functions. Applying the parabola equations, the standard deviations were reduced to half the original values and the mean values are much closer to '1' as shown in Table 6. The equations are determined for the employed lenses to ensure that the predicted error distributions, which are factored by camera-to-object distances, improve JRC estimation using photogrammetry methods.

Table 6
Comparisons of standard deviation and mean values of the normalized JRCs before and after the data reconciliation.

Focal lengths (mm)	Before reconciliation		After reconciliation	
	Standard deviation	Mean	Standard deviation	Mean
24	0.23	0.78	0.13	0.89
50	0.17	0.93	0.09	0.97
85	0.15	0.89	0.08	0.94

8. Conclusions

Close range photogrammetry was employed to investigate the influence of the focal length of employed lenses and the camera-to-object distances for JRC estimation through a set of photogrammetric laboratory tests. Three different focal length lenses (FL=24, 50, 85 mm) were used to extract roughness profiles, as well as JRC values, for up to 7 m of photograph distances. The results recommend allowable photogrammetric distances for the employed focal lengths to produce data with manual measurement precision (at 1 mm intervals). At the allowable distances, the accuracy and precision of JRC data distributions were increased compared to that obtained from the range of distances used in the experiments.

This study developed a quadratic equation which is governed by normalized JRC values and $RMSE_{JRC}$ with camera-to-object distance. The coefficient, a, which is the size of the parabola models, was directly dependent upon the focal lengths of the employed lenses. As a result, the obtained original data from each focal length lens was improved by using each parabola curve. The quadratic equations effectively shifted the biased mean values to the true values and reduced the standard deviations of the data distributions. This study also suggests that the parabola models can be verified and improved by using site photogrammetry data.

Acknowledgments

This research was performed with the financial support of the Griffith University International Postgraduate Research Scholarship (GUIPRS) program. The authors would like to express their appreciation to CSIRO for providing the program SIROVISION for this study.

References

1. Barton N, Choubey V. The shear strength of rock joints in theory and practice. *Rock Mech.* 1977;10:1–54.
2. ISRM. Suggested methods for the quantitative description of discontinuities in rock masses. *Int J Rock Mech Min Sci Geomech Abstr.* 1978;15:319–368.
3. Grasselli G, Wirth J, Egger P. Quantitative three-dimensional description of a rough surface and parameter evolution with shearing. *Int J Rock Mech Min Sci.* 2002;39:789–800.
4. Feng Q, Fardin N, Jing L, Stephansson O. A new method for in-situ non-contact roughness measurement of large rock fracture surfaces. *Rock Mech Rock Eng.* 2003;36(1)3–25.
5. Hong ES, Lee IM, Lee JS. Measurement of rock joint roughness by 3D scanner. *ASTM Geotech Test J.* 2006;26:482–489.
6. Rahman Z, Siefko S, Hack R. *Deriving Roughness Characteristics of Rock Mass Discontinuities from Terrestrial Laser Scan Data.* The Geological Society of London. International Association of Engineering Geology; 2006.
7. Fardin N. Influence of structural non-stationarity of surface roughness on morphological characterization and mechanical deformation of rock joints. *Rock*

Mech Rock Eng. 2008;41:267–297.
8. Fekete S, Diederichs M, Lato M. Geotechnical and operational applications for 3-dimensional laser scanning. *Tunn Undergr Space Technol.* 2010;25:614–628.
9. Tatone BSA, Grasselli G. A new 2D discontinuity roughness parameter and its correlation with JRC. *Int J Rock Mech Min Sci.* 2010;47:1391–1400.
10. Khoshelham K, Altundag D, Ngan-Tillard D, Menenti M. Influence of range measurement noise on roughness characterization of rock surface using terrestrial laser scanning. *Int J Rock Mech Min Sci.* 2011;48:1215–1223.
11. Mah J, Samson C, McKinnon SD, Thibodeau D. 3D laser imaging for surface roughness analysis. *Int J Rock Mech Min Sci.* 2013;58:111–117.
12. Jessell MW, Cox SJD, Schwarze P, Power W. The anisotropy of surface roughness measured using a digital photogrammetric technique. In: Ameen MS, editor. *Fractography: Fracture Topography as a Tool in Fracture Mechanics and Stress Analysis, vol. 92*. Geological Society Special Publication; 1995. p. 27–37.
13. Cravero M, Iabichino G, Ferrero AM. Evaluation of joint roughness and dilatancy of schistosity joints. In: *Proceedings of Eurock 2001*. Espoo; 2001:217–222.
14. Lee HS, Ahn KW. A prototype of digital photogrammetric algorithm for estimating roughness of rock surface. *Geosci J.* 2004;8(3)333–341.
15. Unal M, Yakar M, Yildiz F. Discontinuity surface roughness measurement techniques and the evaluation of digital photogrammetric method. In: *Proceedings of the 20th International Congress for Photogrammetry and Remote Sensing, ISPRS*; 2004:1103–1108.
16. Bistacchi A, Griffith WA, Smith SAF, Di Toro G, Jones R, Nielsen S. Fault roughness at seismogenic depths from LIDAR and photogrammetric analysis. *Pure Appl Geophys.* 2011;168:2345–2363.
17. Sturzenegger M, Stead D. Close-range terrestrial digital photogrammetry and terrestrial laser scanning for discontinuity characterization on rock cuts. *Eng Geol.* 2009;106:163–182.
18. Nilsson M, Edelbro C, Sharrock G. Small scale joint surface roughness evaluation using digital photogrammetry. In: *Proceedings of the Eurock 2012*. Stockholm; 2012.
19. Haneberg WC. Directional roughness profiles from three-dimensional photogrammetric or laser scanner point clouds. In: *Proceedings of the 1st Canada–U.S. Rock Mechanics Symposium*. Vancouver; 2007:101–106.
20. Baker BR, Gessner K, Holden EJ, Squelch A. Automatic detection of anisotropic features on rock surfaces. *Geosphere.* 2008;4(2)418–428.
21. Poropat GV. Remote characterisation of surface roughness of rock discontinuities. In: *Proceedings of 1st Southern Hemisphere International Rock Mechanics Symposium*. Perth; 2008:447–458.
22. Poropat GV. Measurement of surface roughness of rock discontinuities. In: *Proceeding of 3rd CANUS Rock Mechanics Symposium*. Toronto; 2009 [Paper 3976].
23. Poropat GV. Remote 3D mapping of rock mass structure. In: *Proceedings of the Workshop of Laser and Photogrammetric Methods for Rock Face Characterization*. Colorado; 2006:63–75.
24. Kim DH, Gratchev I, Poropat GV. The determination of joint roughness coefficient using three-dimensional models for slope stability analysis. In: *Proceedings of the 2013 International Symposium on Slope Stability in Open Pit Mining and Civil Engineering*. Brisbane; 2013:281–289.
25. Kim DH, Gratchev I, Balasubramaniam AS. Determination of joint roughness coefficient (JRC) for slope stability analysis: a case study from the Gold Coast area, Australia. *Landslides.* 2013;10:657–664.
26. Rengers N. Influence of surface roughness on the friction properties of rock planes. In: *Proceedings of the 2nd Congress of the International Society for Rock Mechanics*. Beograd; 1970:229–234.
27. Fooladgar F, Samavi S, Soroushmehr SMR, Shirani S. Geometrical analysis of localization error in stereo vision systems. *IEEE Sens J.* 2013;13(11)4236–4246.
28. Wolf PR, Dewitt BA. *Elements of Photogrammetry with Applications in GIS*. 3rd ed. Boston: McGraw Hill; 2000:608 p.
29. CSIRO. Field procedures for photogrammetric pit mapping. *CSIRO Exploration & Mining*; 2012.
30. Dai F, Feng Y, Hough R. Photogrammetric error sources and impacts on modelling and surveying in construction engineering applications. *Vis Eng.* 2014;2(2)1–14.
31. Dai F, Lu M. Assessing the accuracy of applying photogrammetry to take geometric measurements on building products. *J Constr Eng Manag.* 2010;136:242–250.
32. Haneberg WC. Using close range terrestrial digital photogrammetry for 3-D rock slope modelling and discontinuity mapping in the United States. *Bull Eng Geol Environ.* 2008;67(4)457–469.
33. Birch JS. Using 3DM analyst mine mapping suite for rock face characterisation. In: *Proceedings of the Workshop of Laser and Photogrammetric Methods for Rock Face Characterization*. Colorado; 2006:13–32.
34. ASPRS. professional practicing division. ASPRS accuracy standards for large-scale maps. *Photogramm Eng Remote Sens.* 1989:1068–1070.
35. Fraser CS. Network design considerations for non-topographic photogrammetry. *Photogramm Eng Remote Sens.* 1984;50(8)1115–1126.
36. Palmström A. *In-situ Characterization of Rocks.* Lise, Abingdon, Exton (PA), Tokio: A.A. Balkema Publishers; 2001.
37. Morelli GL. On joint roughness: measurements and use in rock mass characterization. *Geotech Geol Eng.* 2014;32:345–362.
38. Kim DH, Gratchev I, Balasubramaniam AS. A photogrammetric approach for stability analysis of weathered rock slopes. *Geotech Geol Eng.* 2015;33:443–454 http://dx.doi.org/10.1007/s10706-014-9830-z.
39. Tse R, Cruden DM. Estimating joint roughness coefficients. *Int J Rock Mech Min Sci Geomech Abstr.* 1979;16:303–307.
40. Reeves MJ. Rock surface roughness and friction strength. *Int J Rock Mech Min Sci Geomech Abstr.* 1985;22(6)429–442.
41. Franklin JA, Maerz NH, Bennett CP. Rock mass characterization using photoanalysis. *Int J Min Geol Eng.* 1988;6:97–112.
42. Maerz NH, Franklin JA, Bennett CP. Joint roughness measurement using shadow profilometry. *Int J Rock Mech Min Sci Geomech Abstr.* 1990;27:329–343.
43. Yu X, Vayssade B. Joint profiles and their roughness parameters. *Int J Rock Mech Min Sci Geomech Abst.* 1991;28(4)333–336.
44. Hsiung SM, Ghosh A, Ahola MP, Chowdhury AH. Assessment of conventional methodologies for joint roughness coefficient determination. *Int J Rock Mech Min Sci Geomech Abstr.* 1993;30(7)329–343.
45. Neumann KJ. Trends for digital aerial mapping cameras. In: *Proceedings of the International Archives of the Photogrammetry, Remote Sensing and Spatial Information Sciences*. Vol. XXXVII, Part B1. Beijing; 2008:551–553.